ASTROBIOLOGY
Volume 14, Number 6, 2014

DOI: 10.1089/ast.2013.1100

# Impact-Generated Endolithic Habitat Within Crystalline Rocks of the Haughton Impact Structure, Devon Island, Canada

Alexandra Pontefract,[1] Gordon R. Osinski,[1,2] Charles S. Cockell,[3] Casey A. Moore,[4] John E. Moores,[4] and Gordon Southam[5]

**Abstract**

The colonization of rocks by endolithic communities is an advantageous trait, especially in environments such as hot or cold deserts, where large temperature ranges, low water availability, and high-intensity ultraviolet radiation pose a significant challenge to survival and growth. On Mars, similar conditions (albeit more extreme) prevail. In these environments, meteorite impact structures could provide refuge for endolithic organisms. Though initially detrimental to biology, an impact event into a rocky body can favorably change the availability and habitability of a substrate for endolithic organisms, which are then able to (re)colonize microfractures and pore spaces created during the impact. Here, we show how shocked gneisses from the Haughton impact structure, Devon Island, Canada, offer significant refuge for endolithic communities. A total of 28 gneiss samples representing a range of shock states were analyzed, collected from *in situ*, stable field locations. For each sample, the top centimeter of rock was examined with confocal scanning laser microscopy, scanning electron microscopy, and bright-field microscopy to investigate the relationship of biomass with shock level, which was found to correlate generally with increased shock state and particularly with increased porosity. We found that gneisses, which experienced pressures between 35 and 60 GPa, provide the most ideal habitat for endolithic organisms. Key Words: Endoliths—Impact cratering—Gneiss. Astrobiology 14, 522–533.

## 1. Introduction

The colonization of rocks by microorganisms (referred to as endolithic) has long been documented (Friedmann, 1980) and is seen as an advantageous trait, especially in environments such as hot or cold deserts, where temperature shifts, low water availability, and high UV indices pose a significant problem (Bell, 1993; Cockell *et al.*, 2003; Omelon *et al.*, 2007). In these situations, rocks can provide a refuge for both photosynthetic and chemosynthetic organisms that form complex endolithic communities only millimeters below the surface (Walker and Pace, 2007). The word *endolith* (here encompassing cryptoendoliths) refers specifically to organisms that dwell within the rock with no obvious point of entry and are distinct from epiliths, which are surface-dwelling organisms, and hypoliths that are found on the underside of rocks. Both the porosity and the translucency of the rock have a significant impact on the extent of colonization possible because organisms are dependent on the connectivity of pore spaces (or permeability) beneath the surface as well as the penetration depth of photosynthetically active radiation (PAR) (Walker and Pace, 2007). For this reason, the majority of these communities can be found residing in sedimentary lithologies such as sandstones or in evaporitic rocks such as gypsum and halite, generally 1 mm beneath the surface where the subsurface environment allows for water retention and provides protection from UV radiation (Stivaletta *et al.*, 2010; Wierzchos *et al.*, 2011). The colonization of sandstones in Antarctica has received significant attention (Pointing *et al.*, 2009). In this polar desert, endolithic assemblages can constitute the majority of viable biomass and reproduce at very slow rates with doubling times on the order of thousands of years (Friedmann *et al.*, 1993).

[1]Centre for Planetary Science and Exploration/Department of Earth Sciences, University of Western Ontario, London, Canada.
[2]Department of Physics and Astronomy, University of Western Ontario, London, Canada.
[3]School of Physics and Astronomy, University of Edinburgh, Edinburgh, UK.
[4]Department of Earth and Space Sciences and Engineering, York University, Toronto, Canada.
[5]School of Earth Sciences, University of Queensland, St. Lucia-Brisbane, Australia.

Given that colonization of the endolithic environment is a viable strategy in such extreme conditions, it is plausible that if life existed on other terrestrial bodies in our solar system, such as Mars, these organisms might adopt a similar approach to survival (Wynn-Williams and Edwards, 2000). We cannot be assured, however, that the geological processes that produce lithologies capable of providing endolithic habitats (*e.g.,* quartz-rich sandstones or evaporites) on Earth would operate on other planetary bodies. Meteorite impacts are one mechanism that occurs throughout our solar system and is a fundamental geological process on all rocky and icy planetary bodies (Napier and Clube, 1979; Melosh, 1989; Osinski and Pierazzo, 2013). Though initially detrimental to biology, an impact event can favorably change the availability and habitability of a substrate for endolithic organisms, which can then colonize microfractures and pore spaces created during the impact (Cockell *et al.*, 2002; Cockell, 2006). In these instances, impact structures could provide refuge for endolithic organisms. Cockell and Osinski (2007) showed that the increase of microbial biomass with increasing exposure to shock pressure in sedimentary targets was related to corresponding increases in porosity and translucency. During an impact event, however, the opening of pore spaces is transient, and sedimentary targets experience a collapse of pore spaces at pressures over 35 GPa (Cockell and Osinski, 2007). Thus, they do not support endolithic colonization at pressures higher than this. This is not the case for other substrate types. Singleton *et al.* (2011) showed that, unlike sedimentary targets, the porosity of crystalline samples (specifically gneisses) increases until vaporization, creating a habitat where none previously existed.

Early work by Cockell *et al.* (2002), Cockell (2004), and Fike *et al.* (2003) revealed that shocked gneisses do indeed provide a unique and viable habitat for endoliths, providing a moisture-retaining and UV-protected environment. This is of significant relevance for astrobiology, as opposed to the existence of endolithic habitats in shocked sedimentary rocks, due to the dominance of crystalline rocks on all other terrestrial planets in the Solar System. Seminal work by Cockell *et al.* (2002) investigated the degree of light penetration as well as UV protection between low-shock and high-shock samples of gneiss, where the degree of shock was denoted by the absence of amphibole banding at high pressure. The study revealed that within the high-shock class of samples the light penetration depth at 680 nm—the absorption maximum for chlorophyll *a*—increased by an order of magnitude. Despite this, however, it was shown that 1 mm of the shocked gneiss was capable of reducing spore inactivation in *Bacillus subtilis* by UV radiation by 2 orders of magnitude. Work by Fike *et al.* (2003) looked at the heterotrophic community of these rocks as well as nutrient availability and was the first to note a potential loss of biologically relevant elements. Pontefract *et al.* (2012) showed that bioessential element nutrient availability in these crystalline lithologies does decrease with increasing shock level, though not significantly enough to inhibit microbial growth. The question then is, does microbial biomass trend with this increase in porosity, or are there other factors that determine abundance? To answer this question, we performed a detailed analysis of light transmission within the substrate and employed a multifaceted approach of conducting cell counts, along with scanning electron microscopy (SEM) and confocal scanning laser microscopy (CSLM). Through this, we reveal the morphology and extent of subsurface growth as well as ''hot spots'' of *in situ* microbial growth.

## 2. Methods

### 2.1. Field site

The Haughton impact structure is located in the northwestern region of Devon Island, Nunavut, in the Canadian High Arctic archipelago at 75°08′N, 87°51′W (Osinski *et al.*, 2005a). Haughton was formed approximately $39 \pm 2$ Ma (Sherlock *et al.,* 2005), though a recent study based on radiogenic $^4$He has placed this value closer to $22 \pm 2.0$ Ma (Young *et al.,* 2013). It has an apparent diameter of $\sim$23 km, with a final crater rim estimate of 16 km in diameter (Osinski *et al.*, 2005b). The target rocks are almost entirely sedimentary and represent lower Paleozoic rocks of the Arctic Platform. This $\sim$1880 m sequence (preimpact thickness) is composed of marine carbonates, with lesser amounts of evaporites, sandstone, and shale, that overlie gneisses of the Precambrian basement of the Canadian Shield. The most identifiable feature of the impact structure is the pale gray crater-fill (clast-rich impact melt rocks) deposits (Fig. 1a, 1b), which form a discontinuous layer throughout the center of the structure and have a maximum thickness today of $\sim$125 m, covering $\sim$60 km$^2$ (Osinski *et al.*, 2005b). Another salient feature of the structure is the hydrothermal deposits, seen in the form of several alteration products, such as selenite and marcasite, as well as the presence of hydrothermal vugs (Osinski *et al.*, 2001, 2005a).

### 2.2. Sample collection and processing

Samples of shocked gneiss were collected during the seasons of 2008 and 2010 from $\sim$50 locations within the crater on several of the impact melt rock hills located both near the crater rim and toward the central uplift (Fig. 1b, 1d), coordinates for which are listed in the Supplementary Material (Table S1, available online at www.liebertonline.com/ast). A notation of which surfaces were exposed was also made where possible. Each sample was thin sectioned and studied under a petrographic microscope (Nikon Eclipse LV100POL compound petrographic microscope) to determine shock level, which corresponds to a given pressure range. This was necessary in order to correlate the amount of growth seen in the rocks with the pressure to which the rocks were exposed. In the present study, we used the classification system created by Singleton *et al.* (2011) to assign shock, as well as the estimated porosity values for each shock level (Table 1). It should be noted that in this paper broad terms that refer to shock are sometimes used; that is, ''unshocked'' refers to shock level 0 samples (*e.g.,* Fig. 3a), ''low shock'' to shock levels 1–2, ''moderate shock'' to levels 3–4 (*e.g.,* Fig. 3b), ''high shock'' to shock levels 5–6 (*e.g.,* Fig. 3c), and ''very high shock'' to level 7 samples (*e.g.,* Fig. 3f).

### 2.3. Transmission of photosynthetically active radiation

Transmission measurements were made of the individual rock samples between 400 and 800 nm with an Ocean Optics Red Tide visible/near IR spectrometer validated with a

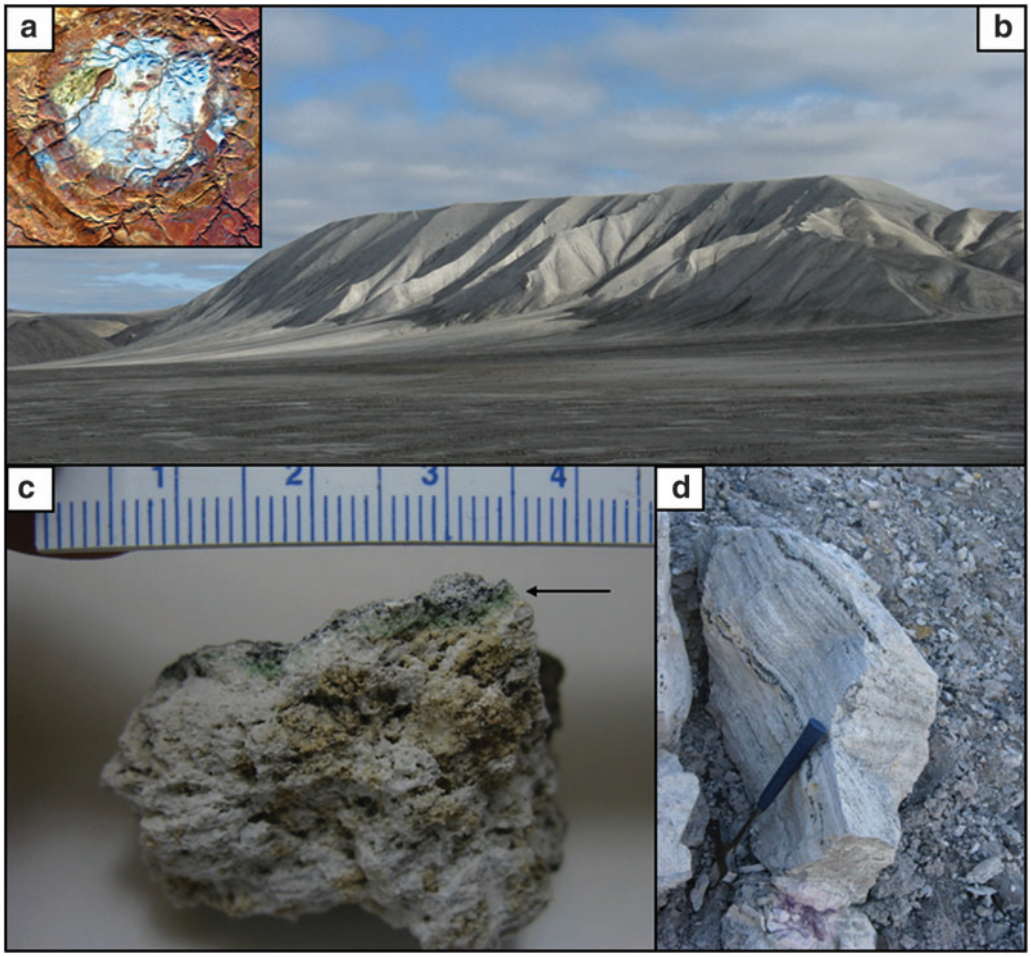


**FIG. 1.** (**a**) Landsat image of Haughton Crater, Devon Island, Canada, courtesy of G.R. Osinski. (**b**) Bruno Escarpment, a breccia hill located southwest in the crater, approximately 1 km in length. (**c**) Fragment of shocked gneiss used for embedding in CSLM and SEM imaging. Endolithic band is visible 1–2 mm beneath the surface (arrow); scale is in centimeters. (**d**) Example of large gneiss breccia within the crater, Easting for scale. (Color images available online at www.liebertonline.com/ast)

Maya 2000 Pro UV and HR 4000 NIR spectrometer at each end of the spectrum. To obtain transmission spectra, a 600 $\mu$m diameter fused silica optical fiber was run from the spectrometer onto a solar tracking platform provided by the York University Observatory. The fiber was terminated with an Ocean Optics 6.35 mm diameter spectralon cosine corrector in order to obtain measurements of the entire downwelling flux, incorporating both direct transmission and scattering within the samples. As such, this work is comparable to that of Cockell *et al.* (2002).

The rock samples tested (three unshocked, four moderate-shock, and four high-shock) were mounted flush with the end of the cosine corrector housing, and the entire rig was pointed at the Sun. Dark spectra, acquired to correct for electrical and thermal noise on the detector, were obtained by disconnecting the spectrometer from the fiber and covering the input aperture of the spectrometer. Light spectra, corresponding to 100% transmission, were obtained by removing the sample. The final downwelling transmitted flux was obtained by subtracting off the dark spectra that correspond to each of the light and sample spectra and then rationing the resulting dark-corrected sample spectra to the dark-corrected light spectra. The values of this downwelling transmission are shown graphically in Fig. 2. For reference, this figure also shows an ASTM G173 standard 1.5 airmass spectrum (ASTM, 2012) normalized at its peak wavelength. At the time and location of acquisition, the airmass factor was approximately 1.8.

### 2.4. Scanning electron microscopy

Samples of shocked gneiss were either fractured into small pieces with a sterile technique and imaged directly with secondary electrons or were embedded in plastic for back-scattered electron microscopy (SEM-BSE) and electron dispersive spectroscopy (EDS). Fractured pieces were fixed in glutaraldehyde, dehydrated in ethanol and critical-point dried to preserve membrane structure, platinum coated with a Denton Vacuum Desk II sputter coater at 12 mA for 150 s, and imaged. For embedded samples, subsamples from each field sample that measured approximately 1–2 $cm^3$ were broken off with a sterile chisel and hammer. These subsamples were then split in half by using the same sterile

Table 1. Classification of Shock Level in Gneisses Based on Petrographic Analysis along with Observations from Microscopic and Confocal Images and Scanning Electron Micrographs, Adapted from Pontefract *et al.* (2012) and Singleton *et al.* (2011)

| *Shock stage* | *Pressure range (GPa)* | *Rock features, mineral effects, and colonization potential* | *Average porosity (%)* |
|---|---|---|---|
| 0 | — | Unshocked substrate. Colonization is purely epilithic. | 0.5 |
| 1 | 2–5 | Beginning of fracturing. Formation of shatter cones and kink banding in biotite. Colonization is epilithic. | n/a |
| 2 | 5–10 | Extensive planar fracturing (PF), along with distinctive checkerboard pattern in plagioclase. Colonization is epilithic. | 1 |
| 3 | 10–30 | The first microscopic deformations begin to form within quartz as planar deformation features (PDFs), along with a toasted appearance and phase transitions of quartz to stishovite. Macrofractures are extensive at this stage. Colonization is still mainly epilithic but with some infilling within the first 1000 $\mu$m of the rock. | 1.5 |
| 4 | 30–35 | Extensive PDF formation, loss of pleiochroism in biotite. Shatter cones are now no longer present. Quartz transitions to coesite also with optically homogeneous extinction. Colonization is still mainly epilithic but with some infilling within the first 1000 $\mu$m of the rock. | 10.5 |
| 5 | 35–55 | Diaplectic glass formation begins (mineral outline still present) to vesiculated glass and partial melting. Loss of extinction in quartz and loss of PDFs. Endolithic colonization is extensive down to 4 mm in depth at the upper end of the pressure range. | 18.5 |
| 6 | 55–60 | Significant vesicularization of the substrate and the beginning of flowed glass features in both quartz and feldspars. Biotite is absent. Endolithic colonization is extensive throughout all samples. | 44.0 |
| 7 | 60–80 | Complete melting of all minerals along with visible flow and differentiation of mafic and felsic materials; connections between pore spaces begin to close. Endolithic colonization is still extensive within the first 1000 $\mu$m but is not readily present at other depths except near the presence of macrofractures. Complete vaporization of rocks past 80 GPa. | 63.0 |

Porosity values were calculated from raw data from Singleton *et al.* (2011) and are used as the estimated porosity for samples in this study.

technique to expose an inner cross section of the rock. The entire sample was then fixed in 2% glutaraldehyde for 24 h and then rinsed for 15 min in a Na-cacodylate buffer. Samples were then stained by using a 0.1 *M* $OsO_4$-cacodylate buffer for 1 h. An acetone dehydration series was performed (15 min each at 50%, 75%, and 100%), followed by two rinses at 15 min of 100% acetone. Samples were then embedded with EMbed following the protocol from Electron Microscopy Sciences (Hattfield, PA) and Dykstra and Reuss (2003). The osmium tetroxide serves as a lipid membrane stain and makes imaging of cells possible when using electron back-scattering (SEM-BSE).

### 2.5. Bulk cell counts

For each shock level, excepting levels 1 and 2 (which were omitted due to the scarcity of samples available from within the crater), three samples were selected for bulk cell counts. Because the cell counts of the endolithic community solely were to be tallied, any surface crust that could possibly be housing epilithic communities was removed with a sterile pick and chisel under a dissecting scope. Samples were then hand crushed to a fine sand grain size with an alumina mortar and pestle (CoorsTek, CO, #60370). One gram of sample was then suspended in 20 mL of a 5 m*M* sodium pyrophosphate solution (Haldeman *et al.*, 1993; Hirsch *et al.*, 1995; Buss *et al.*, 2003), vortexed briefly, and then sonicated on low power for 5 min. Five hundred microliters of the solution was then suspended in 1 mL $dH_2O$ and counted with a Petroff-Hausser stage in a Zeiss Axio Imager Z1 microscope with a 40× objective. Counts of five different grids were conducted based on methods from Hausser Scientific used to determine the total cell number in a 1 $mm^2$ field of view. The total number of cells in the initial volume was then calculated and divided by the total number of grams of rock for the given sample to achieve a value in cells per gram.

### 2.6. Confocal scanning laser microscopy

A total of 14 samples were analyzed with CSLM and consisted of two unshocked, two low-shock, four moderate-shock, four high-shock, and two very high–shock in order to visualize *in situ* microbial colonization of the rocks and as an analysis of levels of biomass. Embedded samples were first prepared with the same methodology as for the SEM samples to expose an inner cross section of the rock. For imaging endolithic cells *in situ*, a method was adapted from de los Ríos *et al.* (2005) and Wierzchos *et al.* (2004). The fresh rock surface was stained with LIVE/DEAD *Bac*Light L7007 from Invitrogen (Molecular Probes, Eugene, OR). This is a fluorescent stain that contains two types of nucleic binding fluorophores: SYTO 9, which is membrane-permeable and will bind to the nucleic acids in all cells, and a propidium

iodide (PI) counterstain, which is restricted to cells with damaged membranes. Two hundred microliters of the mixture was pipetted onto the fresh surface and incubated in the dark at room temperature for 1 h. Each sample was then fixed in 2% glutaraldehyde for 1 h, dehydrated with ethanol (15 min each at 50%, 75%, 100%, and 100%), and then embedded in resin (LR White, Electron Microscopy Sciences, Hattfield, PA) by using the cold cure method from Electron Microscopy Sciences. These cured pucks were then polished and mounted for imaging. The unshocked samples were used as the control, as an unshocked crystalline rock was presumed to only have epilithic (surface) growth, which was confirmed with microscopic observations.

### 2.7. Confocal scanning laser microscope image acquisition and processing

For each puck, representing one sample, three transects of the rock were taken with a CSLM (Zeiss LSM 5 Duo, software: Zen 2009 v.5.5 SP2) from the top of the sample (exterior face) to the bottom (interior face), representing an increase in depth, at 20× magnification, with a sampling volume having a depth of 1.9 $\mu$m. This magnification was used because higher magnification did not allow for the necessary working distance with the sample; it did, however, satisfy the Nyquist-Shannon sampling theorem (Marks, 1986), where 2 pixels represented 0.88 $\mu$m in this instance. Images were acquired by using three lasers: green fluorescence (SYTO 9/live stain) with excitation/emission of 488/510–530 nm with an argon laser; red fluorescence (PI/dead stain) with excitation/emission of 543/620–750 nm with a HeNe laser; and rock surface reflectance was imaged with a 633 HeNe laser. Images were processed with Image Pro (v.7.0), wherein each transect was tiled and then split into its respective channels (*i.e.,* Rock, SYTO 9, and PI) for enumeration. The rock channel was used as a representation of background noise and subtracted from the SYTO 9 and PI channels. Bins of 500 $\mu$m in length (with a constant area of 150,000 $\mu$m) were constructed and overlaid on each transect channel to count pixels (corresponding with individual cells) for both SYTO 9 and PI channels, respectively. These counts were then averaged to provide an overall approximation for cellular abundance with increasing depth for each rock type.

## 3. Results

### 3.1. Transmission of photosynthetically active radiation

Transmission of samples ranged from a few percent for high-shock samples up to just over 30% at 800 nm for unshocked rocks (Fig. 2). In general, samples tended to be more transmissive at longer wavelengths, with no sample above 10% transmission at 400 nm and three samples above 20% transmission at 800 nm. Furthermore, the effect of heterogeneity was significant, especially within the unshocked and highly shocked samples. Each sample consisted of a combination of minerals with very different transmissivities. As such, different transmission values could be obtained depending on the geographic location on the sample where the fiber was directed. In practice, for the size of cosine corrector used, this difference in transmission could vary up to a factor of 4 for samples with especially transmissive mineralogies. Where samples contained holes, as in the high-shock samples, the region of study on the sample was selected to minimize the number and size of these holes. This gives a transmissivity of the rock itself that, for a known pore number density and area, can be used to determine the transmittance of a given sample. This type of effect was observed most strongly for one of the high-shock samples for which the transmittance was as low as a few percent where holes were not present (Fig. 2, red dashed line) and as high as 30% in areas with significant porosity (Fig. 2, light blue dashed line).

Experiments were also conducted by using an in-laboratory spectrophotometric technique that measured the transmission of plane-parallel light through samples. The advantage of this setup is that only light that passes through the samples without scattering is transmitted to the receiving spectrometer. This allows us to investigate the relative proportion of light scattered versus the amount of light that passes through the rock without scattering. In these experiments, it was found that well in excess of 99% of light passing through the rocks interacted with the rock, even for the thinnest samples.

### 3.2. Scanning electron microscopy

Scanning electron microscope imaging revealed a clear progression of shock within the samples, correlated with microbial growth. Figure 3a shows a SEM-BSE image of unshocked gneiss collected from Sverdrup Inlet outside the crater. At this stage, the rock is very cohesive, and only minor epilithic growth is generally observed, with the potential for chasmoendolithic infiltration, especially by lichens. Increasing in pressure exposure, Fig. 3b shows a moderately shocked sample with extensive epilithic growth. At this stage, large macrofractures occur within the substrate that allow for the infiltration of meteoric water and nutrients, which can sometimes support chasmoendolithic communities, though this is not extensively observed at this shock level. In some cases, these epilithic communities did not infiltrate the rock subsurface due to the presence of a weathering layer (data not shown). Figure 3c, 3d, 3e shows increasing magnification of the same area for a high-shock sample, where the substrate has been exposed to approximately 50 GPa of pressure. At this stage, massive melt and flow of the substrate is observed, along with a significant increase in porosity. Many of the minerals have formed a diaplectic glass, where grain boundaries are still visible. In these samples, cryptoendolithic growth is observed between 0.5 and 3 mm beneath the surface, sometimes visibly seen as a coherent green band in the subsurface. The colony depicted in Fig. 3c, 3d is located 1 mm beneath the surface and shows both coccoid cyanobacteria and rod-shaped bacteria. Figure 3e shows a close-up of the area indicated in 3d, in which the relationship of the cells to each other and the presence of extracellular polymeric substances can be seen. Based on the lipid staining quality of $OsO_4$ (Glauert, 1975), the strong white regions in these back-scattered electron images are interpreted as lipid storage granules (see Wältermann and Steinbüchel, 2005). Finally, Fig. 3f shows a highly shocked sample, which was exposed to over 60 GPa in pressure. The rocks at this stage are almost entirely in a

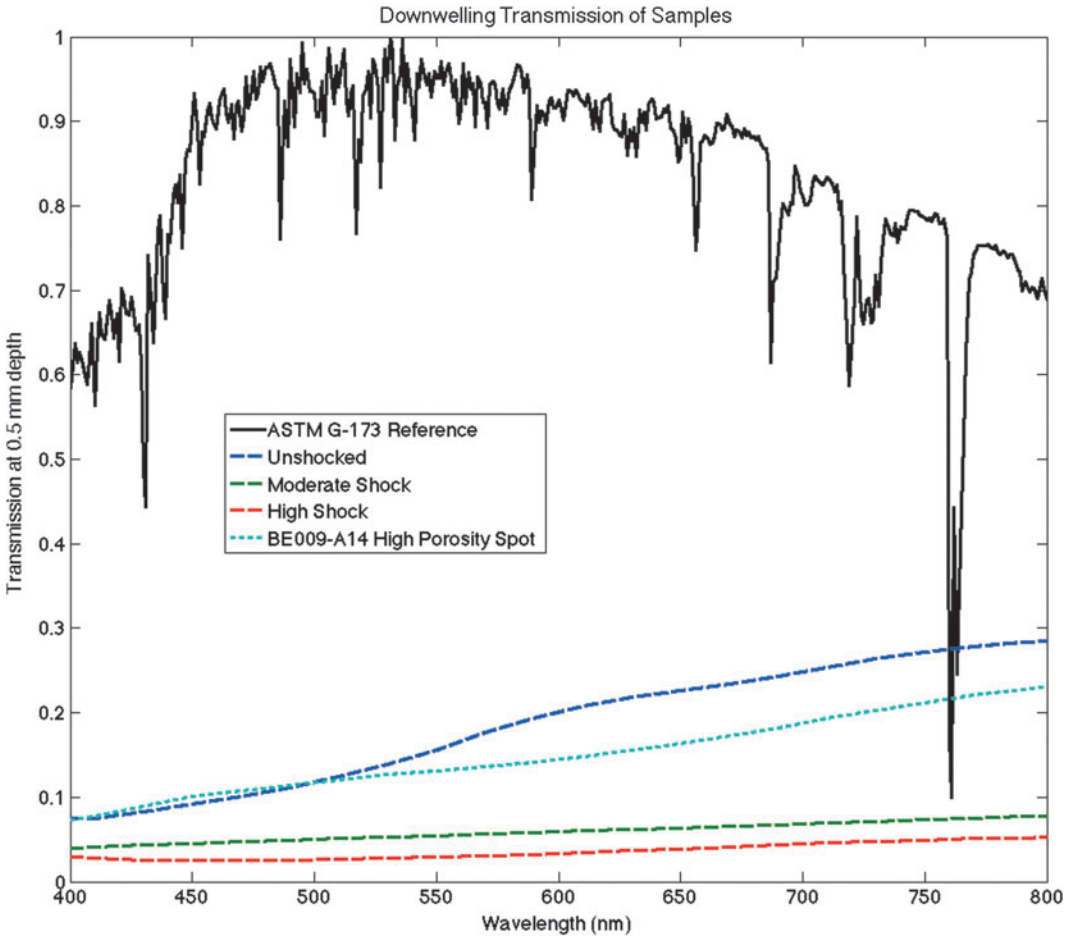


**FIG. 2.** Downwelling transmission of samples (spectral flux at 0.5 mm compared to spectral flux at 0 mm). The spectrum of sunlight is shown in black, with the colored lines indicating the mean transmissivity of different shock-level samples tested, with the exception of BE009-A14 (light blue), which represents a single data set. Most samples are more transmissive at longer wavelengths, indicating that PAR can penetrate to deeper depths within the rock. All samples used were 0.5 mm samples except for one of the moderately shocked samples, which was a 1 mm sample. (Color images available online at www.liebertonline.com/ast)

glass phase and are highly porous and friable. Little or no cryptoendolithic growth is observed in these instances, and much of the growth is either epilithic or chasmoendolithic. The dark pore spaces seen in 3f, as indicated by the arrow, are void spaces within the rock that were not able to be infilled during the embedding process, revealing low connectivity at this shock level.

### 3.3. Bulk cell counts

Results for bulk microbial cell counts from shocked gneisses are shown in Fig. 4. Shock level 0 values begin at $10^7$ cells/g, representing surface (epilithic) growth, and then increase by an order of magnitude at shock levels 2–4, increasing again past shock level 4. A linear regression was fit to the data, having an $R^2$ value of 0.92. A fourth-order polynomial was also fit to the data with an $R^2$ of 0.97. Both regressions were compared for statistical significance by using the Akaike information criterion, and the linear regression was found to have a better goodness of fit for the data, though the difference was negligible.

### 3.4. Confocal scanning laser microscopy

Confocal scanning laser microscope images can be seen in Fig. 5. In all cases, growth from the epilithic community was observed to continue into the rocks, following fissures and fractures within the rock (Fig. 5), with the outermost layer typically containing dead or damaged cells (red fluorescence) (Fig. 5b). Figure 5c is an example of one of the constructed confocal transects, from which the data for Fig. 6 was gathered. Figure 6a gives a comparison of total microbial biomass for each category, showing that the high-shock samples (levels 5 and 6) have the highest overall biomass in comparison with the other samples. This data fits a linear correlation with an $R^2$ of 0.61, with the Akaike criterion again showing that the linear fit was negligibly more significant than the polynomial. Figure 6b shows average cell number with increasing depth and increasing shock level. In this instance, shock levels have been grouped into broader categories, as use of the previously mentioned fine scale was not able to reveal growth trends within the samples. The first data point indicates a range of 0–500 $\mu$m

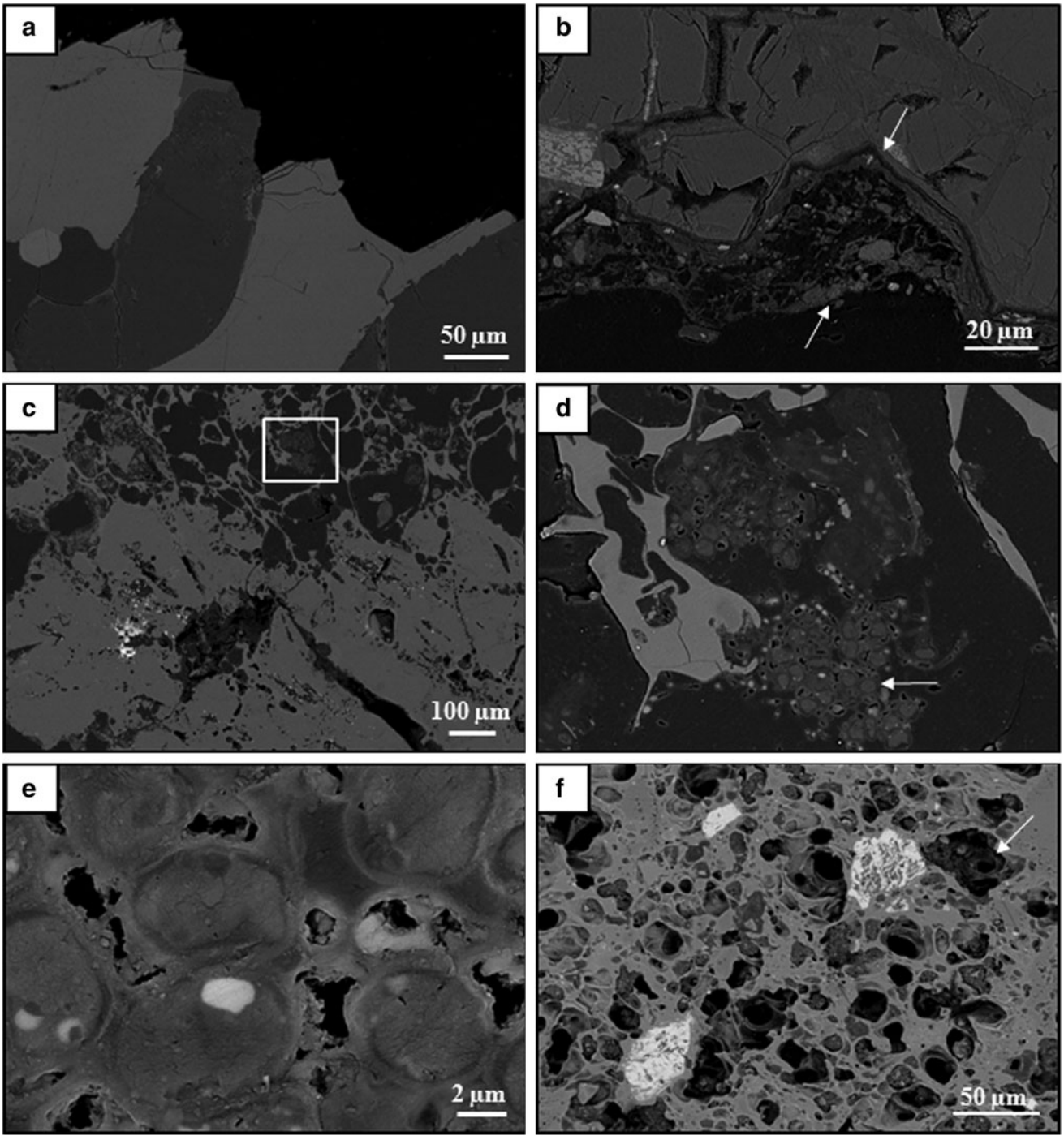


**FIG. 3.** SEM-BSE micrographs of endolithic organisms within shocked gneiss. (**a**) Unshocked gneiss collected from Sverdrup Inlet. No endolithic growth occurs at this stage. Epilithic growth is intermittent or absent, as in this micrograph. (**b**) Gneiss exposed to between 10 and 30 GPa showing fractures. Arrows bound the epilithic growth, which is the primary form of colonization at this stage, though chasmoendolithic growth is observed. (**c**) Zoom-out of lithic substrate shocked to ~50 GPa. Square shows area of zoom-in for (d) and (e). (**d**) Endolithic colony. Arrow indicates area of zoom-in for (e). Darker region between the rock and colony is the embedding resin. Lighter color encapsulating the colony is extracellular polymeric substances. (**e**) Micrograph showing cocci, possessing concentrated zones of osmium (*i.e.,* the white spots), which presumably represents lipid storage granules (see Wältermann and Steinbüchel, 2005). (**f**) Gneiss exposed to over 60 GPa. Cryptoendolithic growth is intermittent, and chasmoendolithic growth prevails due to the friability of these rocks. A lack of connectivity between pore spaces is also observed at this stage. Arrow indicates the many dark regions in the micrograph, which are areas unfilled by embedding resin.

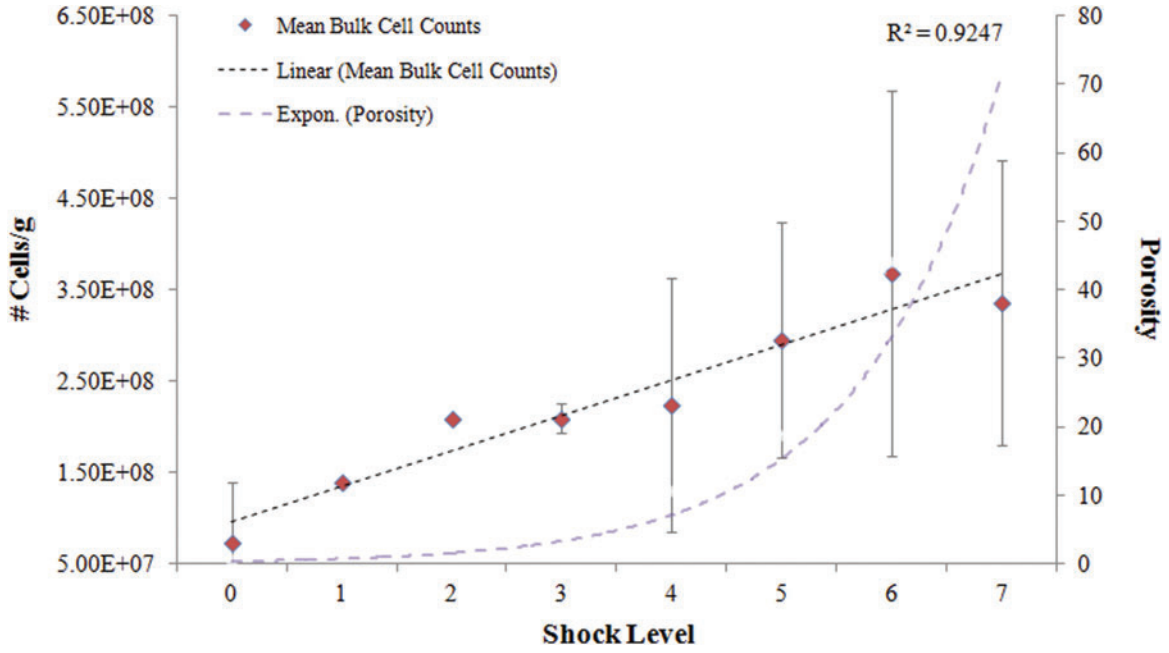


**FIG. 4.** Average number of cells per gram and porosity plotted versus shock level. Dashed line represents the exponential increase seen in porosity for gneisses; data adapted from Singleton *et al.* (2011). Standard deviation values are not shown for shock levels 1 and 2 for cells per gram due to insufficient sample numbers. Grain density and bulk density were calculated for each sample by using helium pycnometry and a volume displacement method. From this, porosity could then be calculated. (Color images available online at www.liebertonline.com/ast)

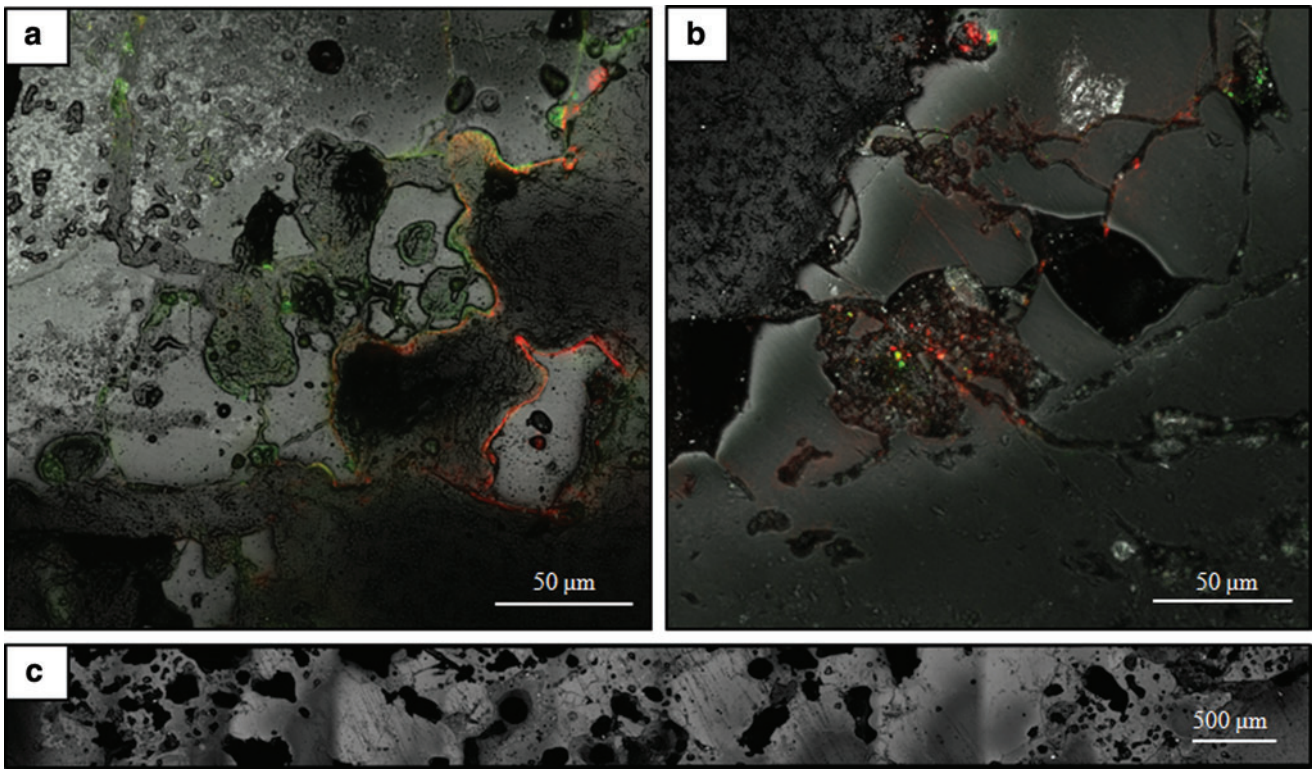


**FIG. 5.** Images (**a** and **b**) show CSLM micrograph with live (green)/dead (red) stain and reveal epilithic and endolithic colonization of fractures and vesicles within the rock. The mottled dark-gray substrate [*e.g.,* (b) top left] is embedding resin. (**c**) A stitched transect in the ''rock'' channel showing extensive porosity and fracturing throughout the sample at shock level 6. (Color images available online at www.liebertonline.com/ast)

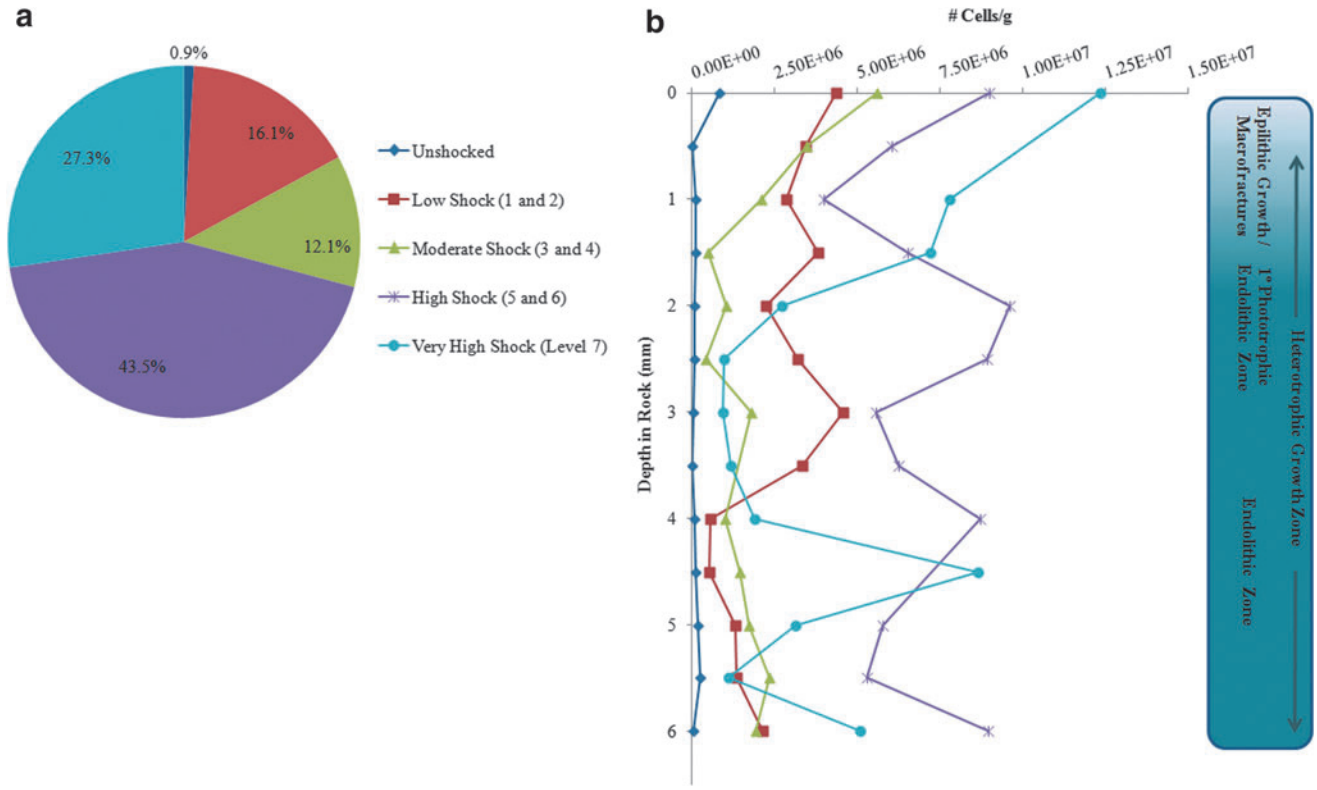


**FIG. 6.** Average number of cells per gram plotted versus shock level (**a**) and depth within the substrate (**b**) through *in situ* analysis. (a) Biomass levels for each shock category, where 100% indicates the total biomass from all samples. (b) Graph shows increasing shock level from left to right and variations with increasing depth. Note that each data point represents a bin sum of 150,000 $\mu m^2$; therefore, the first data point is indicative of surface epilithic growth and growth associated with macrofractures. The primary photosynthetic zone is indicated (right) as well as zones for heterotrophic and epilithic colonization. (Color images available online at www.liebertonline.com/ast)

beneath the surface, and so on with increasing depth. Shock level 0 shows an initial spike in microbial abundance at the surface and then diminishes with increasing depth. The subsequent shock levels show a concomitant increase in biomass, especially within the initial 2 mm of the plot. Shock level 7 (very high shock) shows lower biomass overall than the ''high shock'' samples, though with increased variability, indicated by sharp increases and decreases in abundance values. SEM-BSE images of the same constructed confocal transects (*e.g.,* Fig. 5c) were also taken to provide substrate information for the location of cryptoendolithic colonies. Because of the sheer size of these images, full transects are not shown; instead Fig. 7 shows one tile each of a confocal and back-scattered image for comparison of cell growth versus substrate type.

## 4. Discussion

The Haughton impact initially heated a portion of the target rocks to temperatures in excess of 2000°C (Osinski *et al.,* 2005a), which eventually cooled down with time such that the formation of a hydrothermal system could occur. Over time, the system dissipated and left behind the impact melt rock hills situated within barren Arctic tundra that are observed today (Cockell and Lee, 2002). The microorganisms within these rocks are representative of a contemporary environment (Cockell *et al.*, 2002), though calcified cells are present within the lithology (image not shown). Building on earlier work by Cockell *et al.* (2002), Cockell (2004), and Fike *et al.* (2003), we have provided the first systematic investigation of the relationship between microbial colonization of crystalline rock and level of shock, with samples categorized into seven shock levels—previous studies classified samples as either ''low shock'' or ''high shock.'' It can be seen that the epilithic environment reveals stratification, with dead cells composing the outermost layer, offering protection to the active photosynthetic layer. Inward, cohesive colonization becomes more prevalent with an increasingly shocked target and peaks in the shock level 6 samples (Fig. 4), which corresponds to a pressure exposure of 40–50 GPa and a mean porosity of 44% (Singleton *et al.,* 2011). SEM images also reveal relatively greater levels of colonization (Fig. 3) at these high-shock stages, which is not seen in lower shock level samples. This is similarly reinforced by the CSLM *in situ* counts (Fig. 6), which show a peak in microbial cell abundance at the high-shock range.

### 4.1. Microbial biomass and shock metamorphism

The bulk microbial cell counts for these samples reveal a linear trend with increasing shock metamorphism of the target. There are, however, several factors that control the abundance of biomass for each shock level, such as porosity, permeability, translucency, friability, and substrate type (*e.g.,*

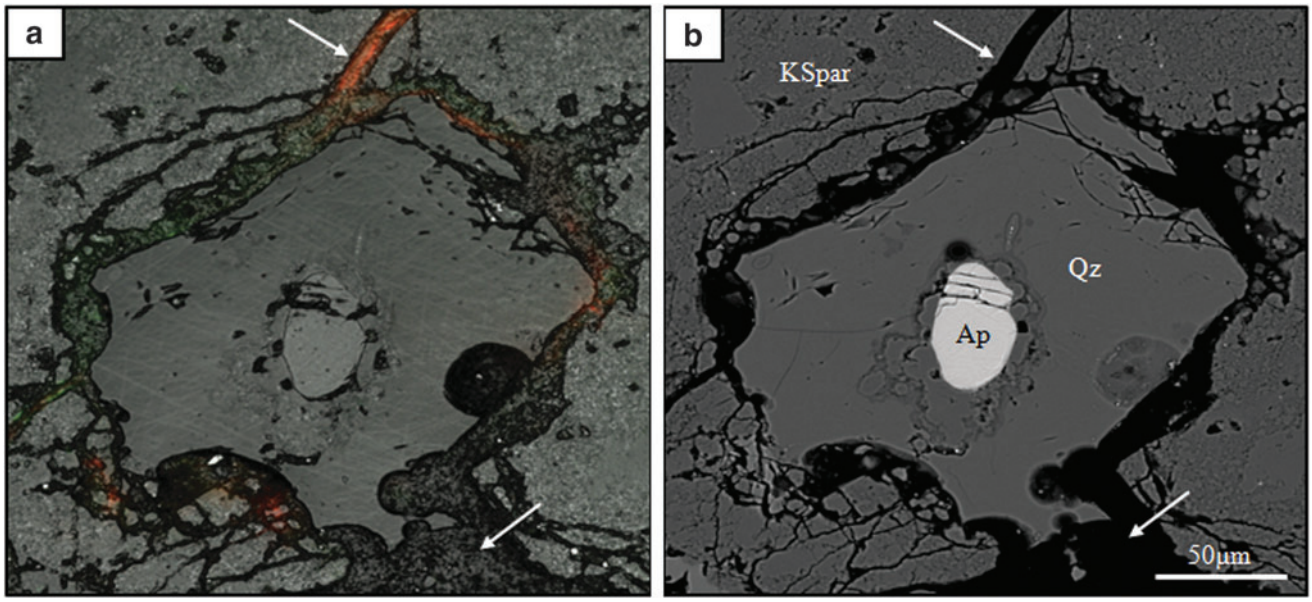


**FIG. 7.** (**a**) CSLM micrograph with *in situ* LIVE/DEAD *Bac*Light stain. Top arrow shows fluorescence of cells with damaged membranes stained with PI, and bottom arrow points to embedding resin. Compare with (**b**), a SEM-BSE micrograph, where both areas indicated in (a) are primarily composed of carbon (embedding resin) and so show up as black in backscatter. Substrate is variable with a feldspathic glass (KSpar), a quartz glass (Qz), and an apatite crystal (Ap). (Color images available online at www.liebertonline.com/ast)

glass vs. crystalline mineral). Though it is possible that these factors combine in such a way as to confer a linear relationship between biomass and shock level, the data also support a more complex multifactored model. When considering the biomass levels in terms of the above-mentioned factors and using a nonlinear fit, two distinct plateaus in the data become apparent. The first plateau occurs over shock levels 2–4, where large-scale macrofractures are occurring in the rock and allow for an increase in chasmoendolithic growth; however, porosity of the substrate is still below 10% of the total bulk volume (see Table 1), and transmittance of PAR is reduced to a few percent that of incident light (Fig. 2). Porosity does not begin to increase rapidly until shock level 5, which corresponds with the next jump in biomass values.

Interestingly, the shock level 7 values dip below that of the previous shock level. Though not a significant difference, *in situ* cell counts also show a corresponding reduction of biomass levels at the highest shock level (Fig. 4a). That both methodologies reveal a concomitant loss of biomass points to something more complex influencing microbial growth at these pressures. One possible hypothesis that would account for this loss in abundance is that, though porosity is increasing rapidly at this stage—going from 44% at shock level 6 to over 60% at shock level 7—what is unknown is the corresponding change in permeability of the rock, where extensive flow of melt within these samples may act to effectively isolate pore spaces. Currently, however, there are no supporting investigations into this phenomenon. Given these notable changes in biomass levels and the several known factors that affect growth, it is likely that the relationship between biomass and shock level is more complex than a linear relationship and that the current data set is too small to reveal such trends.

Though *in situ* imaging with CSLM did not show a strong linear correlation, a polynomial regression for the data revealed a good correlation, and again the linear fit was a negligible improvement over the polynomial when using the Akaike information criterion. Though the data did not fit a linear correlation when using the fine-scale shock classification system, they were significant when grouped into the broader categories used in Fig. 6a, 6b. It is likely that a more robust sample set would more clearly reveal trends in biomass increases; however, given the time-intensive process when using this method, performing bulk cell counts is the preferred method. What the CSLM micrographs did reveal, however, was a clear progression of biomass levels with shock level and the expansion of habitation depth with shock level. In all shocked samples, colonization of the rock down to 2 mm was fairly consistent, and cell numbers increase with shock accordingly. Below this point, however, cell numbers drop by an order of magnitude in all but the high-shock samples, which show a large range in variability with increasing depth likely due to the friability of the substrate and connectivity of pore spaces.

What reveals the importance that porosity plays in microbial subsurface growth, however, is the data from transmittance for PAR. The PAR data shown in Fig. 2 reveal that transmittance actually decreases with increasing shock. This is likely due to the fact that unshocked samples possessed coherent crystals, which did not act to scatter the light significantly. In the moderately and highly shocked samples, metamorphic effects that cause physical breaking of the crystal lattice planes and phase transitions to glasses resulted in a substrate where 99% of the light is scattered and transmission is on the order of a few percent. However, it is at these high-shock levels that we see the greatest

microbial growth. Our study showed that the pore spaces in the samples were 100% transmissive and that porous regions allowed as much as 30% of the incident light through (though this number is dependent on the size of the cosine corrector and is likely an underestimate). This transmitted light must account for the totality of the photosynthetically active microbial communities observed in these shocked lithologies. Furthermore, this correlates with the study conducted by Cockell *et al.* (2002), which shows that highly shocked samples let through approximately 40% of the incident light in the upper end of the visible spectrum and that this is not due to an increase in translucency but rather to the prevalence of extensive pore spaces. Finally, for all samples it was noted that light at longer wavelengths penetrated deeper into the substrate than the shorter, more damaging wavelengths, though UV irradiance would not be mitigated for organisms residing in a pore space receiving 100% transmission of light.

### *4.2. Subsurface morphology*

Using SEM-BSE in conjunction with the CSLM transects (Fig. 7), we were able to correlate areas of growth with substrate type to ascertain whether some substrates, such as feldspathic glasses, may provide increased nutrients to microbial colonies over other possible surfaces. Interestingly, we found that there was no such preference seen over 42 transects studied. It would appear that the microbial colonies within these gneisses are following both macro- and microfractures to the interior of the rock, eventually colonizing the interiors of vesicles. Fike *et al.* (2003) hypothesized that the volatilization process could effectively concentrate bioessential nutrients along the inside of these vesicles, which would allow for increased levels of colonization.

Given that no infiltration of glasses was seen in any of the SEM-BSE and CSLM images, and that much of the glass is quartz-rich, it is unlikely that these impact-formed glasses provide much nutrient to the microbial colonies. In this way, ''hot spots'' of growth that are observed are likely governed by three main factors: (1) the trade-off between the depth of PAR transmission for a given sample versus the ability to act as a sufficient UV shield, the depth of which occurs at 1–2 mm beneath the surface; (2) the connectivity of pore spaces within the rock; and (3) the connectivity of these spaces with macro- and microfractures to the surface, allowing the percolation of pore waters, nutrients, and microbiota. It is possible that, over time, weathering of the substrate could ''reveal'' nutrient-loaded regions of the rock and result in the formation and storage of lipid (Fig. 3d, 3e) granules that would enhance long-term survival. In Fig. 7, for example, we see an apatite crystal surrounded by quartz glass. Given that phosphate can be limiting for microbial ecosystems, these apatite crystals could act as a localized source of nutrients once accessed through microbial weathering processes.

## 5. Concluding Remarks

Based on the results presented in this paper, we find that uniquely generated impact-shocked gneisses provide an excellent habitat for microbial endoliths in harsh environmental conditions. We see that microbial biomass levels reach maximum values within gneisses exposed to between 55 and 65 GPa and that more highly shocked targets may not be as suitable a habitat due to potential losses in the permeability of the rock at such high pressures. In our opinion, understanding how biology correlates with shock in gneisses from a well-preserved crater will give us a better understanding of how it might respond in other crystalline targets such as basalts. In our current work, we endeavor to address that very question. Given the dominance of shocked crystalline lithologies on every terrestrial body in the Solar System, it is plausible that, if life existed elsewhere, endolithic colonization of impact craters would have occurred beyond Earth. On Mars, many of these shocked lithologies are buried under multiple layers of ejecta, are protected from high levels of UV radiation and low atmospheric pressures, and could provide an excellent target for future life-detection missions.

## Acknowledgments

This work was funded by the National Sciences and Engineering Research Council, the Canadian Astrobiology Training Program, and the Northern Scientific Training Program, with logistical support provided by the Polar Continental Shelf Program. Thank you to Karen Nygard and Integrated Microscopy @ Biotron for CSLM support, as well as Todd Simpson and Tim Goldhawk from the Nanofabrication Laboratory and Ivan Barker and the Zap Lab for SEM and EDS support. Thank you also to Phil McCausland, Chris Omelon, Asuncion de los Ríos, and Jeremiah Shuster for their help and logistical advice, and Alaura Singleton and Jenine McCutcheon for their field support. Finally, all authors thank the two anonymous reviewers for their valuable commentary and insights regarding this manuscript.

## Author Disclosure Statement

No competing financial interests exist.

## Abbreviations

CSLM, confocal scanning laser microscopy, confocal scanning laser microscope; EDS, electron dispersive microscopy; PAR, photosynthetically active radiation; PI, propidium iodide; SEM, scanning electron microscopy, scanning electron microscope; SEM-BSE, back-scattered electron microscopy, back-scattered electron microscope.

## References

ASTM. (2012) *Standard Tables for Reference Solar Spectral Irradiances: Direct Normal and Hemispherical on 37° Tilted Surface,* ASTM G173-03(2012), Book of Standards Vol. 14.04, ASTM International, West Conshohocken, PA, doi:10.1520/G0173-03R12.

Bell, R.A. (1993) Cryptoendolithic algae of hot semiarid lands and deserts. *J Appl Phycol* 29:133–139.

Buss, H.L., Brantley, S.L., and Liermann, L.J. (2003) Non-destructive methods for removal of bacteria from silicate surfaces. *Geomicrobiol J* 20:25–42.

Cockell, C.S. (2004) Impact-shocked rocks—insights into archaean and extraterrestrial microbial habitats (and sites for prebiotic chemistry?). *Adv Space Res* 33:1231–1235.

Cockell, C.S. (2006) The origin and emergence of life under impact bombardment. *Philos Trans R Soc Lond B Biol Sci* 361:1845–1856.

Cockell, C.S. and Lee, P. (2002) The biology of impact craters—a review. *Biol Rev Camb Philos Soc* 77:279–310.

Cockell, C.S. and Osinski, G.R. (2007) Impact-induced impoverishment and transformation of a sandstone habitat for lithophytic microorganisms. *Meteorit Planet Sci* 42:1985–1993.

Cockell, C.S., Lee, P., Osinski, G.R., Horneck, G., and Broady, P. (2002) Impact-induced microbial endolithic habitats. *Meteorit Planet Sci* 37:1287–1298.

Cockell, C.S., McKay, C.P., and Omelon, C.R. (2003) Polar endoliths—an anti-correlation of climatic extremes and microbial diversity. *International Journal of Astrobiology* 1:305–310.

de los Ríos, A., Wierzchos, J., Sancho, L.G., Green, T.G., and Ascaso, C. (2005) Ecology of endolithic lichens colonizing granite in continental Antarctica. *The Lichenologist* 37:383–395.

Dykstra, M.J. and Reuss, L.E. (2003) *Biological Electron Microscopy: Theory, Techniques and Troubleshooting,* 2nd ed., Kluwer Academic/Plenum Publishers, New York, pp 1–31, 86, 101.

Fike, D.A., Cockell, C.S., Pearce, D., and Lee, P. (2003) Heterotrophic microbial colonization of the interior of impact-shocked rocks from the Haughton impact structure, Devon Island, Nunavut, Canadian High Arctic. *International Journal of Astrobiology* 1:311–323.

Friedmann, E.I. (1980) Endolithic microbial life in hot and cold deserts. *Orig Life* 10:223–235.

Friedmann, E.I, Kappen, L., Meyer, M.A., and Nienow, J.A. (1993) Long-term productivity in the cryptoendolithic microbial community of Ross Desert, Antarctica. *Microb Ecol* 25:51–69.

Glauert, A. (1975) Fixation, dehydration and embedding of biological specimens. In *Practical Methods of Electron Microscopy,* Vol. 3, Part I, American Elselvier Publishing Company, Inc., New York, pp 5–19.

Haldeman, D.L., Amy, P.S., Ringelberg, D., and White, D.C. (1993) Characterization of the microbiology within a 21 $m^3$ section of rock from the deep subsurface. *Microb Ecol* 26:145–159.

Hirsch, P., Eckhardt, F.E.W., and Palmer, R.J., Jr. (1995) Methods for the study of rock-inhabiting microorgansims—a review. *J Microbiol Methods* 23:143–167.

Marks, R.J. (1986) Multidimensional-signal sample dependency at Nyquist densities. *J Opt Soc Am A Opt Image Sci Vis* 3:268–273.

Melosh, H.J. (1989) *Impact Cratering: A Geologic Process,* Oxford University Press, London, pp 60–86.

Napier, W.M. and Clube, S.V.M. (1979) A theory of terrestrial catastrophism. *Nature* 282:455–459.

Omelon, C.R., Pollard, W.H., and Ferris, F.G. (2007) Inorganic species distribution and microbial diversity within High Arctic cryptoendolithic habitats. *Microb Ecol* 54:740–752.

Osinski, G.R. and Pierazzo, E. (2013) Impact cratering: processes and products. In *Impact Cratering: Processes and Products,* edited by G.R. Osinski and E. Pierazzo, Blackwell Publishing, Oxford, pp 1–20.

Osinski, G.R., Spray, J.G., and Lee, P. (2001) Impact-induced hydrothermal activity within the Haughton impact structure, Arctic Canada: generation of a transient, warm, wet oasis. *Meteorit Planet Sci* 36:731–745.

Osinski, G.R., Lee, P., Parnell, J., Spray, J.G., and Baron, M. (2005a) A case study of impact-induced hydrothermal activity: the Haughton impact structure, Devon Island, Canadian High Arctic. *Meteorit Planet Sci* 40:1859–1877.

Osinski, G.R., Lee, P., Spray, J.G., Parnell, J., Lim, D.S.S., Bunch, T.E., Cockell, C.S., and Glass, B. (2005b) Geological overview and cratering model for the Haughton impact structure, Devon Island, Canadian High Arctic. *Meteorit Planet Sci* 40:1759–1776.

Pointing, S.B., Chan, Y., Lacap, D.C., Lau, M.C.Y., Jurgens, J.A., and Farrell, R.L. (2009) Highly specialized microbial diversity in hyper-arid polar desert. *Proc Natl Acad Sci USA* 106:19964–19969.

Pontefract, A., Osinski, G.R., Lindgren, P., Parnell, J., Cockell, C.S., and Southam, G. (2012) The effects of meteorite impacts on the availability of bioessential elements for endolithic organisms. *Meteorit Planet Sci* 47:1681–1691.

Sherlock, S., Kelley, S., Parnell, J., Green, P., Lee, P., Osinski, G.R., and Cockell, C.S. (2005) Re-evaluating the age of the Haughton impact event. *Meteorit Planet Sci* 40:1777–1787.

Singleton, A.C., Osinski, G.R., McCausland, P.J.A., and Moser, D.E. (2011) Shock-induced changes in density and porosity in shock-metamorphosed crystalline rocks, Haughton impact structure, Canada. *Meteorit Planet Sci* 46:1774–1786.

Stivaletta, N., López-García, P., Boihem, L., and Millie, D.F. (2010) Biomarkers of endolithic communities within gypsum crusts (Southern Tunisia). *Geomicrobiol J* 27:101–110.

Walker, J.J. and Pace, N.R. (2007) Endolithic microbial ecosystems. *Annu Rev Microbiol* 61:331–347.

Wältermann, M. and Steinbüchel, A. (2005) Neutral lipid bodies in prokaryotes: recent insights into structure, formation, and relationship to eukaryotic lipid depots. *J Bacteriol* 187:3607–3619.

Wierzchos, J., de los Ríos, A., Sancho, L.G., and Ascaso, C. (2004) Viability of endolithic micro-organisms in rocks from the McMurdo Dry Valleys of Antarctica estabilished by confocal and fluorescence microscopy. *J Microsc* 216:57–61.

Wierzchos, J., Cámara, B., de los Ríos, A., Davila, A.F., Sánchez Almazo, I.M., Artieda, O., Wierzchos, K., Gómez-Silva, B., McKay, C., and Ascaso, C. (2011) Microbial colonization of Ca-sulfate crusts in the hyperarid core of the Atacama Desert: implications for the search for life on Mars. *Geobiology* 9:44–60.

Wynn-Williams, D.D., and Edwards, H.G.M. (2000) Antarctic ecosystems as models for extraterrestrial surface habitats. *Planet Space Sci* 48:1065–1075.

Young, K., van Soest, M.C., Hodges, K.V., Watson, E.B., Adams, B.A., and Lee, P. (2013) Impact thermochronology and the age of Haughton impact structure, Canada. *Geophys Res Lett* 40:3836–3840.

Address correspondence to:
*Alexandra Pontefract*
*Department of Earth Sciences*
*University of Western Ontario*
*1151 Richmond Street*
*London, ON N6A 5B7*
*Canada*

*E-mail:* apontefr@uwo.ca

Submitted 11 September 2013
Accepted 4 April 2014